HiSST: 2nd International Conference on
High-Speed Vehicle Science & Technology
11-15 September 2022, Bruges, Belgium

Design of axisymmetric contoured nozzles for calorically and thermally imperfect gases using the HYPNOZE code

Guillaume Grossir[1] *and Olivier Chazot*[2]

Abstract

A design methodology for supersonic and hypersonic contoured axisymmetric nozzles in presence of real gas effects is presented. The design approach relies on the method of characteristics and includes both dense gas effects and high-temperature effects. The implementation of the methodology relies on tabulated flow properties issuing from appropriate equations of state. Inviscid contours are determined from piecewise velocity and Mach number polynomials prescribed along the nozzle axis. The design of the transonic contour in presence of real gas effects is carefully addressed and a solution is presented to fulfill the continuous wall curvature requirements. The influence of a real gas equation of state on the contours of axisymmetric nozzles is presented. The corresponding design tool "HYPNOZE" also includes design methods for the convergent, features corrections for viscous effects, and enables efficient parametric studies.

Keywords: *nozzle design, axisymmetric, contoured, transonic, supersonic, hypersonic, method of characteristics, design parameters, perfect gas, real gas, equation of state, dense gases*

Nomenclature

Latin

a – speed of sound, m/s
A – area, m^2
$A,\ B,\ C,\ D...$ – points identified in Fig. 1
c_p – specific heat capacity at constant pressure, J/(kg.K)
c_v – specific heat capacity at constant volume, J/(kg.K)
d^* – nozzle throat diameter, m
h – specific enthalpy, J/kg
K^2 – nozzle discharge coefficient
l – length, m
M – Mach number
n – iteration index
p – pressure, Pa
r – distance from the source of a radial flow, m
r^* – nozzle throat radius, m
r_{cr} – distance r in a radial flow for which M=1, m
R – ratio of throat radius of curvature to throat radius
R_c – throat radius of curvature, m
Re – Reynolds number
T – temperature, K
V – flow velocity, m/s
$x,\ y$ – Cartesian coordinates, m
X_{BC} – dimensionless distance between points B and C, $X_{BC} = \frac{x_C - x_B}{r_{cr}}$
W – reduced velocity
Z – compressibility factor

Greek

γ – specific heat ratio
δ – boundary layer thickness, m
δ^* – boundary layer displacement thickness, m
θ – flow angle, degrees
μ – Mach angle, degrees
ρ – density, kg/m^3
$\bar{\Psi}$ – dimensionless stream function
ω – nozzle opening angle, degrees

Superscripts

* – sonic flow properties

[1] *Senior Research Engineer, von Karman Institute for Fluid Dynamics, Rhode-Saint-Genèse, Belgium, grossir@vki.ac.be*
[2] *Professor and Head of Department, von Karman Institute for Fluid Dynamics, Rhode-Saint-Genèse, Belgium, chazot@vki.ac.be*

Subscripts
0 – stagnation flow condition
∞ – free-stream flow properties
core – dimensions of the core flow
exit – flow properties at the nozzle exit
ref – based on Eckert's reference conditions

1. Introduction

1.1. Framework

The method of characteristics has been introduced in the late 1920s [1] in order to design supersonic nozzles. Improvements have been brought over the years [2–5], but the mathematical foundation remains unaltered. Numerous textbooks describe this theoretical method [6, 7], with the axisymmetric case being reported for instance by [5, 8].

Regardless of the nozzle type (either 2-dimensional or axisymmetric), the methodology followed to determine an inviscid contour usually starts from a Mach number distribution (or pressure, or velocity...) imposed along the nozzle axis (from the sonic line near the throat, up to the apex of the uniform flow region) and the condition of a uniform parallel flow by the nozzle exit. Such a procedure rapidly becomes computationally intensive when designing high Mach numbers nozzles, i.e. when large area ratios are required. For axisymmetric designs, a radial flow region was introduced by [9] within the nozzle in order to reduce the computational domain in which the method of characteristics needs to be applied. Within this radial region, the flow is expanding uniformly from a source located upstream, and local flow properties along its boundaries can be derived and serve as boundary conditions to the method of characteristics applied to the adjacent regions. This approach was improved further [4, 10] to avoid curvature discontinuities along the contour leading to the general nomenclature illustrated in Fig. 1.

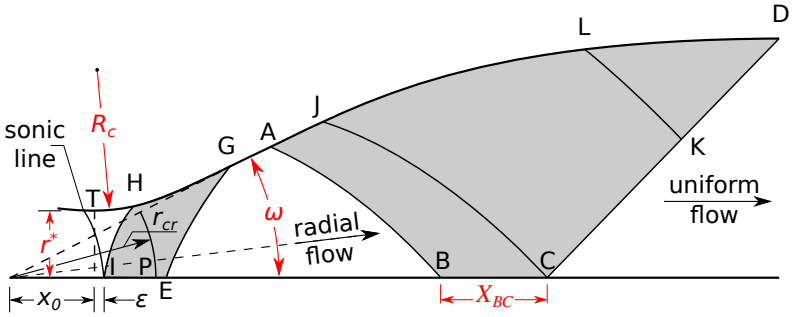

Fig 1. Nomenclature used for the design of an axisymmetric nozzle [4], with the radial flow region bounded by the points EGAB.

One-dimensional isentropic expansion computations show that the ratio of specific heats γ strongly influences the area-ratio requirements to reach prescribed flow conditions. High-temperature and high-pressure effects both influence the isentropic exponent and the method of characteristics therefore needs to account for such variations. This has been accounted for by a few authors. A first approach distinguishes the nozzle expansion upstream of the radial flow region (i.e. region bounded by IEGH) from the one taking place downstream (region bounded by ABCD), by using one specific heat ratio γ within each region [11]. This approach neglects variations of the thermodynamic properties during the initial rapid expansion that may influence the determination of the inviscid contour. As an alternative, the flow properties in the upstream region may be determined using a one-dimensional real gas code [12, 13] (possibly accounting for finite rate chemistry), while the flow composition in the downstream region is again assumed to be frozen and where the usual method of characteristics for a calorically perfect gas is then employed. Other approaches rely on a variable isentropic exponent [14] or tabulated thermodynamic properties [15, 16] while applying the method of characteristics across both regions upstream and downstream of the radial flow region.

1.2. Motivation

The objective of the present work is to ease the design of axisymmetric nozzles in presence of both high-temperature and dense gas effects. The corresponding HYPNOZE code (initially developed for the design of HYPersonic NOZzlEs but applicable to supersonic Mach numbers as well) which has been developed for this purpose is described hereafter together with its main features.

2. Nozzle design methodology and code features

2.1. Nozzle design parameters

There exists an infinite number of nozzle contours which yield, theoretically, the same uniform exit flow conditions. In practice, among all theoretical designs available, some offer better performances than others and the nozzle design parameters need to be selected cautiously. The four major design parameters used by the method of [5], as implemented in the present HYPNOZE code, are listed hereafter, together with some recommendations about the typical values to be used:

- The ratio $\frac{R_c}{r^*}$, where R_c is the throat radius of curvature and r^* is the nozzle throat radius. As reported in [17], a value of $\frac{R_c}{r^*} = 1$ is recommended as an absolute minimum for accurate machining and the use of values as large as possible is advised in order to achieve the best flow quality. There is actually a weak influence of this design parameter on the overall nozzle dimensions, as indicated by parametric studies.
- The maximum nozzle opening angle ω. Small deflection angles ω avoid disastrous flow separation. Numerous nozzles were designed with $8\,^\circ \leq \omega \leq 12\,^\circ$. Hypersonic quiet nozzles designed to maintain laminar boundary layers during the flow expansion rely on even shallower opening angles (e.g. $4\,^\circ$ [18]). Shallow opening angles require longer nozzles to reach a prescribed Mach number, but this usually benefits to the uniformity of the flow across the nozzle exit [17] and limits the growth of Görtler vortices in the specific case of quiet nozzles.
- The length between points B and C (Fig. 1), namely X_{BC}, which characterizes the transition region between the end of the radial flow region and the beginning of the uniform one. From a physical point of view, it is important to note that the Mach number distribution in between points B and C is actually driven by the portion of the contour in between points A and J. The latter points belong to the theoretical inviscid contour. Due to the unavoidable presence of viscous effects in real configurations, it is of interest to maximize the aspect ratio $\frac{\overline{AJ}}{\delta^*_{AJ}}$ (where δ^*_{AJ} is the mean value of the boundary layer displacement thickness along this portion of the contour) in order to achieve the proper gradual compression of the flow. In practice, choosing a Mach number at point B in between 75 and 80% of the Mach number at point C leads to a satisfactory length in between points A and J [5]. It also eases its accurate machining.
- The scaling factor r_{cr}. Coordinates for the nozzle designs are initially scaled by this parameter corresponding to the distance at which the flow becomes supersonic in a radial flow expansion. Inviscid nozzle designs can then be scaled to any dimension to match for instance a prescribed nozzle throat diameter d^*.

2.2. Tabulated flow properties

The thermodynamic flow properties of a gas undergoing an isentropic expansion from prescribed stagnation flow conditions (pressure p_0, and temperature T_0) are determined using either a perfect gas or real gas equation of state. Typical flow properties (pressure p, temperature T, density ρ, enthalpy h, speed of sound a, velocity u, specific heats c_p and c_v, compressibility factor Z...) are tabulated for different free-stream Mach number and serve as an input to the nozzle design code. For sufficient accuracy, tables are typically based on constant pressure steps $p_{n+1} = 0.999 p_n$ until the flow has expanded to Mach numbers sufficiently large to enable the nozzle design.

The real gas equation of state currently implemented in HYPNOZE follows the state-of-the-art equations recommended by NIST, and is based on the Helmholtz energy of the fluid. The one used for nitrogen is described by [19]. Similar equations could be implemented for other gas species.

2.3. Radial flow region

The interest of introducing a radial flow region bounded by EGAB (Fig. 1) is that the local flow properties within this domain can be determined without resorting to the method of characteristics. The equations describing a steady three-dimensional radial flow expansion (i.e. from a point source) in the absence of viscosity and heat transfer are given by [2]:

$$\left(1 - M^2\right) \frac{dV}{dr} + 2\frac{V}{r} = 0 \tag{1}$$

where r is the distance from the source, M is the local Mach number, and V is the local flow velocity. This equation can be solved either for a perfect gas equation of state or a real gas one, and enables to tabulate all quantities of interest for any reduced distance $\frac{r}{r_{cr}}$, together with their derivatives with respect to the reduced distance (r_{cr} being the critical distance from the source at which the flow Mach number is equal to 1).

The left-running characteristic line issuing from E, and the right-running one passing by B, can both be determined from the integrated characteristic equations given by [15]. Their extremities, identified as points A and G, are defined as the intersections with the radius passing by the origin of the source flow and inclined with an angle ω (the maximum opening angle of the nozzle). The flow properties along these characteristic lines are then simply determined as a function of the reduced distance $\frac{r}{r_{cr}}$ from the source using the tabulated flow properties defined earlier, and will be used as boundary conditions for the method of characteristics.

2.4. Stream function

A reduced stream function $\bar{\Psi}$ for an axisymmetric compressible flow is defined by eq. 2 [2]:

$$\bar{\Psi} = \int_0^s \frac{\rho}{\rho_0} W \sin\mu \frac{y}{{r_{cr}}^2} ds \tag{2}$$

where W corresponds to the reduced flow velocity, and μ is the local Mach angle. The limiting value $\bar{\Psi}_{\max}$ for this stream function will serve to identify the streamline corresponding to the inviscid contour when using the method of characteristics. This limiting value can be obtained from eq. 2 applied within the radial flow region in which the flow properties are constant for a given distance from the source. Using flow properties readily available at point A (bounding the radial flow region), this simplifies to eq. 3.

$$\bar{\Psi}_{\max} = \frac{\rho_A}{\rho_0} W_A \left(\frac{r_A}{r_{cr}}\right)^2 (1 - \cos\theta_A) \tag{3}$$

2.5. Method of characteristics and boundary conditions

The formulation of the method of characteristics for the axisymmetric case is given as follows [8]:

$$\left.\begin{aligned} \left.\frac{dy}{dx}\right|_+ &= \tan(\theta + \mu) && \text{(4a)} \\ \frac{dV}{V} - \tan\mu d\theta &= \frac{\tan\mu \sin\mu \sin\theta}{\cos(\theta + \mu)} \frac{dx}{y} && \text{(4b)} \end{aligned}\right\} \text{for left-running characteristics}$$

$$\left.\begin{aligned} \left.\frac{dy}{dx}\right|_- &= \tan(\theta - \mu) && \text{(5a)} \\ \frac{dV}{V} + \tan\mu d\theta &= \frac{\tan\mu \sin\mu \sin\theta}{\cos(\theta - \mu)} \frac{dx}{y} && \text{(5b)} \end{aligned}\right\} \text{for right-running characteristics}$$

where V is the local flow velocity, θ is the local flow angle, and μ is the local Mach angle. The intersection of the two families of characteristics and the local flow properties at that location are determined by solving eqs. 4 and 5. The numerical implementation in HYPNOZE follows the one used by [5]. In presence of real gas effects, the isentropic exponent is influenced, which in turns alters the local speed of sound and, as a consequence, the Mach angle μ appearing in eqs. 4a and 4b. This is accounted for in the present case using the flow properties tabulated earlier (§2.2).

Boundary conditions are prescribed along boundaries IEG and ABCD (Fig. 1). The velocity polynomial imposed along the segment IE and the Mach number polynomial imposed along the segment BC follow the recommendations of [5] in order to ensure continuity of the first and second derivatives of the flow properties with the transonic, radial, and exit regions. Flow properties along the left-running characteristic line EG, and along the right-running characteristic line AB, are obtained from tabulated flow properties characterizing the radial flow expansion from a point source (§2.3). The last characteristic line CD bounds the uniform and parallel core flow region where the flow properties are constant.

Computations in the domain ABCD are initiated next to point C (Fig. 1). The method of characteristics enables to determine where characteristic lines belonging to different families intersect each other and which are the local flow properties at this location. For improved accuracy, an iterative procedure involving the flow properties at that intersection is used until convergence to a prescribed degree of accuracy is achieved. The method then progresses along a left-running characteristic line in a stepwise manner towards point D until the value of the local stream function exceeds the limiting value $\bar{\Psi}_{max}$ of the inviscid wall streamline (eq. 3). An accurate location of the inviscid wall is then determined from a cubic interpolation knowing the evolution of the stream function all along the characteristic. The method is repeated until the whole domain ABCD is meshed.

A similar methodology is used to determine the inviscid contour in between points G and H, and all flow properties within the domain IEGH. By the end of this procedure the inviscid supersonic contour of the nozzle is completed (Fig. 2), at the exception of the transonic region adjacent to the throat (in between points T and H, Fig. 1).

2.6. Transonic contour

The design of the contour in the transonic region for a perfect gas can be achieved using a circular arc, a parabola or a hyperbola following the method described in [20, 21].

When a real gas equation of state is involved, this approach is however no longer suitable as it leads to undesirable discontinuities on the nozzle contour derivatives near point H. An example is shown in Fig. 3 where identical design parameters have been used to obtain inviscid nozzle contours (apart from the equation of state). This figure shows that circular arcs for the transonic contour would no longer match the supersonic contour obtained from the method of characteristics. In particular, the first and second derivatives at point H differ from the ones of the supersonic contour. The reason for such a discrepancy is due to the rapid expansion of the flow through the nozzle that is influencing the local isentropic exponent of the gas. This alters the geometry of the inviscid contour as determined from the method of characteristics. Note that the location of point I, E and others also differ slightly, due to the variations of the isentropic exponent in the real gas case.

An alternative approach has therefore been implemented in order to determine the transonic contour whenever a real gas equation of state is involved. In this case, a second order polynomial is fitted to the supersonic contour over a short distance downstream of point H with the additional constraints that it must pass precisely through point H and match the first derivative at this point. With this approach, the location of the throat (point T) is no longer defined by the transonic solution of [20], but is instead determined from the parabola providing the best fit with the beginning of the supersonic contour. It also meets the continuity requirements for the contour on the first and second derivatives at point H.

This procedure involves a curve fitting technique whose associated uncertainties can be estimated by applying it to a perfect gas case and comparing the results with the theoretical solution obtained for the throat location defined by [4, 20]. Axial, radial and absolute deviations from this theoretical solution

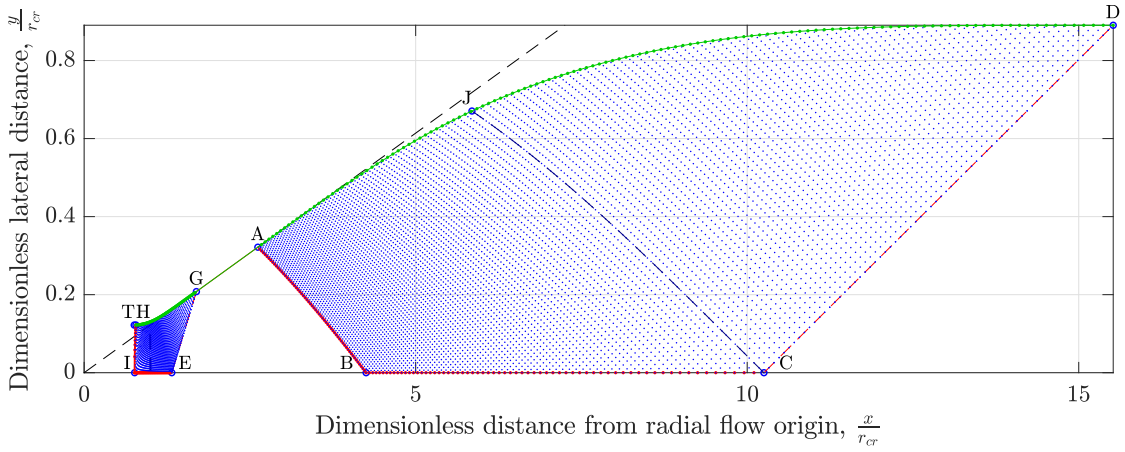

(a) $\gamma = \frac{7}{5}$, yielding the expected area ratio of $\frac{A_{\text{exit}}}{A^*} = 53.179$ for Mach 6.

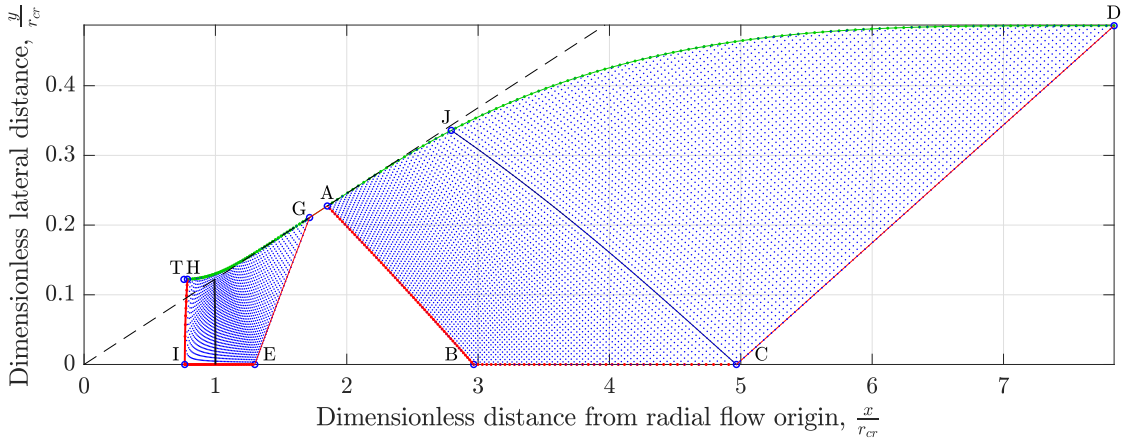

(b) $\gamma = \frac{5}{3}$, yielding the expected area ratio of $\frac{A_{\text{exit}}}{A^*} = 15.84$ for Mach 6.

Fig 2. Example of inviscid contours for Mach 6 axisymmetric nozzles obtained for perfect gases (ω =7°, R=30 and $X_{BC} = 6$).

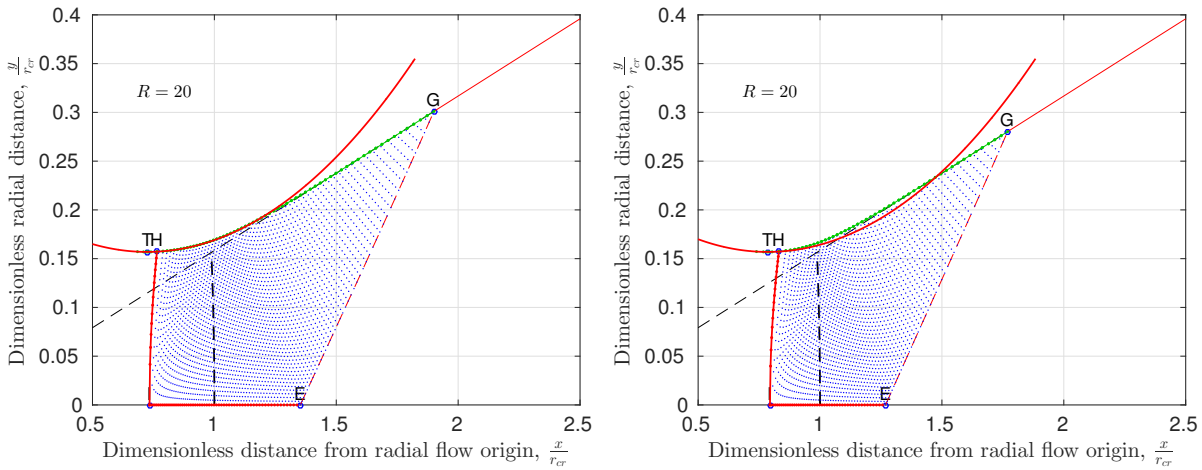

(a) Perfect gas case.

(b) Real gas case.

Fig 3. Transonic solution in the throat region for different equations of state obtained for identical nozzle design parameters ($R = \frac{R_c}{r^*} = 20$).

(taking the origin of the radial flow as a reference) are indicated in Fig. 4a for a perfect gas case as the ratio $R = \frac{R_c}{r^*}$ is increased. Results show that the larger the ratio R, the more accurate the radial location of the throat (y_T). This is a consequence of the shorter distance between points T and H (as the ratio R increases) over which the contour needs to be extended. For $R \geqslant 8$, radial deviations are under 0.16%, and drop to 0.001% for $R > 20$ showing that the accuracy of the method is excellent. Slightly larger errors are observed on the axial location of the throat (smaller than 0.45% for $R > 10$) but are less of a concern since they do not influence the nozzle mass flow rate.

When applied to a real gas case, the accuracy of this methodology can be estimated instead from mass flow considerations knowing that the same mass flow passes through the nozzle throat and through the nozzle exit. Flow properties at the throat are taken as sonic flow conditions (readily available from tabulated real gas isentropic flow expansion). The resulting mass flow ratio is then expressed by eq. 6 where the nozzle discharge coefficient K^2 accounts for the curvature of the sonic line [4]. The corresponding deviations on the nozzle throat diameter are indicated in Fig. 4b as the value of R is increased. Results show that the use of a polynomial performs well for values of $R \gtrsim 10$. Deviations on the throat radius y_T from an ideal radius ensuring mass flow conservation, fall below 0.8% for $R = 8$) and 0.008% for $R > 20$. This shows that the transonic contour can be approximated from a polynomial when a real gas equation of state is used, provided large values of R are used. Typical transonic contours resulting from this approach are shown in Fig. 5 for $R = 5$, 10 and 30. The benefits of using large R values when designing real gas nozzles is obvious from these figures as the distance between points H and T reduces.

$$\frac{\dot{m}^*}{\dot{m}_{\text{exit}}} = \frac{\rho^* u^* \pi {r^*}^2 K^2}{\rho_{\text{exit}} u_{\text{exit}} A_{\text{exit}}} \tag{6}$$

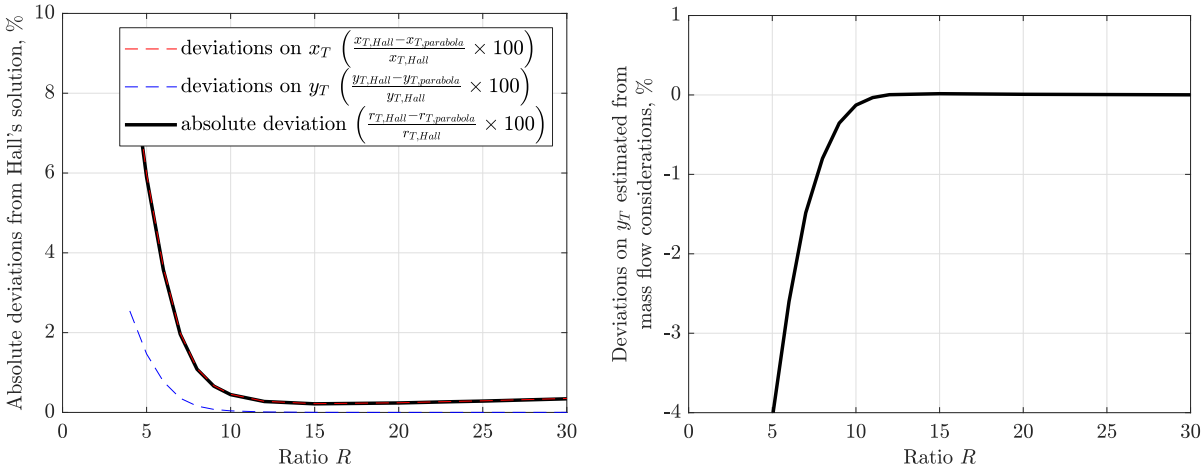

(a) Results evaluated for perfect gas designs, using the reference throat location obtained from [4, 20].

(b) Results evaluated for real gas designs, based on mass flow considerations.

Fig 4. Estimation of uncertainties associated with the use of a second order polynomial for the transonic contour.

2.7. Upstream nozzle convergent

A literature survey shows that the upstream convergent leading to the nozzle throat can be designed using several different approaches. Sivells [5] uses a conical section surrounded by two quartic polynomials (i.e. a Cylinder-Quartic-Cone-Quartic method). The main advantage of this approach is that the maximum slope for the convergent can be specified directly by the user. It also matches the throat flow profile assumed by the nozzle design procedure [17]. Korte [11] describes the use of a conical (or wedge) inlet approaching a circular contour at the throat using exponential functions. Craddock [22]

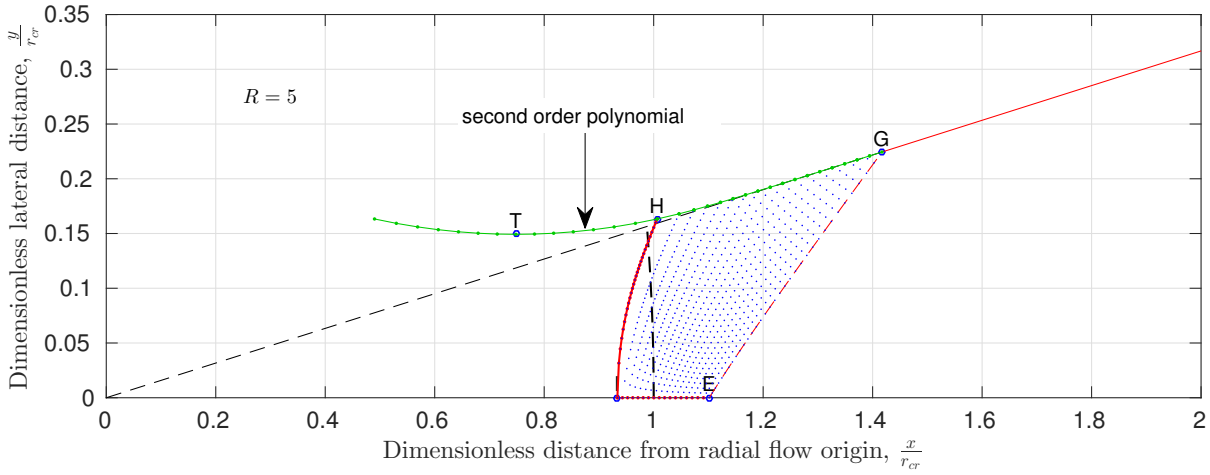

(a) $R = 5$.

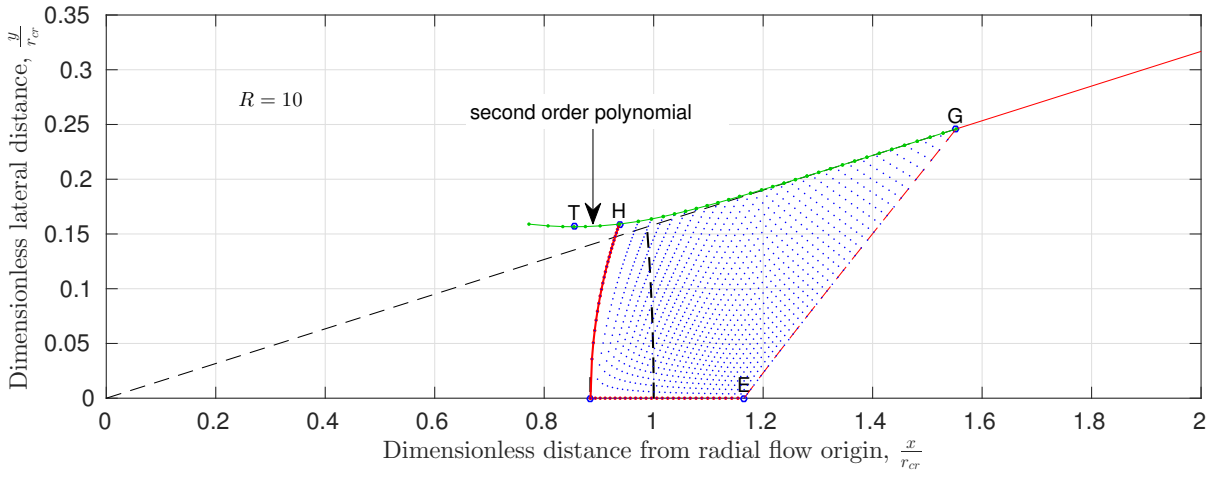

(b) $R = 10$.

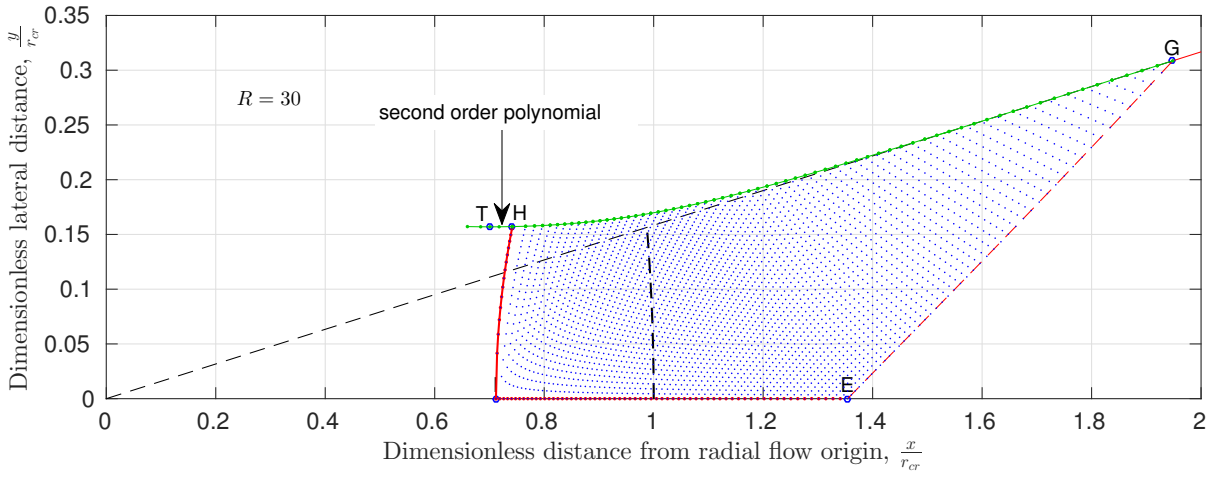

(c) $R = 30$.

Fig 5. Real gas (N_2, $p_0 = 220$ MPa, $T_0 = 2000$ K) transonic contours following a second order polynomial and matching the first and second derivatives of the existing supersonic contour at point H.

relies on Bezier curves with control points chosen as to ensure local continuity with the contour next to the throat. Further results reported by [23] indicate that large inflection angles and curvature discontinuities upstream of the throat do not significantly alter the nozzle flow uniformity as long as the curvature at the throat is continuous.

The Cylinder-Quartic-Cone-Quartic method is implemented in HYPNOZE. As an alternative, 5th order polynomial can be used and also guarantees continuity of the contour curvature from the inlet of the convergent up to the throat.

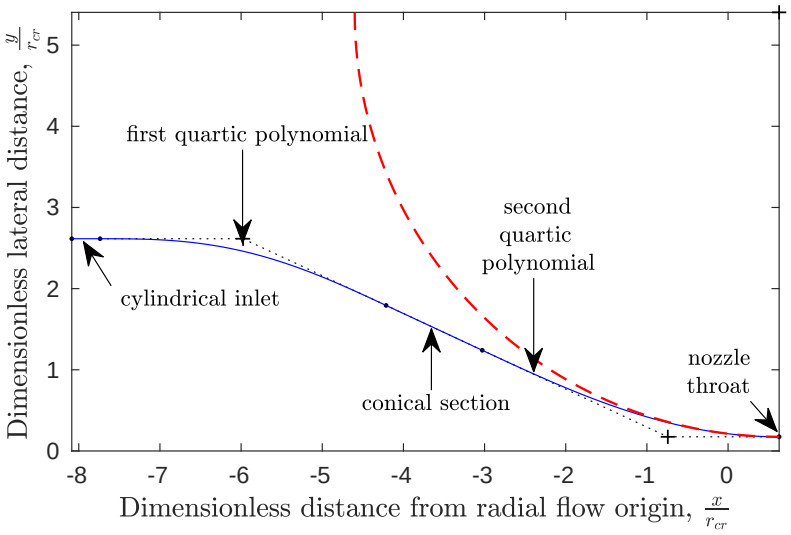

Fig 6. Design of the convergent following the method described by [17].

2.8. Viscous correction and nozzle length optimization

Viscous effects are responsible for the development of boundary layers along the nozzle walls. With the exception of quiet tunnels, which are specifically designed to maintain laminar boundary layers along their nozzle walls [24–26], boundary layer instabilities (e.g. Görtler [27]) promote transition to turbulence and lead to turbulent side wall boundary layers.

Viscous corrections are required to account for the presence of either laminar or turbulent side wall boundary layers. Integral methods have been used previously [5, 28] as well as empirical correlations. The ones established by Edenfield [29] for turbulent boundary layers (eqs. 7 and 8) developing within contoured nozzles operating between $10^3 < Re_{\text{ref}} < 10^7$ and $5 < M < 22$, enable to quickly estimate the magnitude of the viscous effects along the nozzle contour:

$$\frac{\delta}{x} = 0.195 \frac{M^{0.375}}{Re_{\infty,\,x}^{0.166}} \tag{7}$$

$$\frac{\delta^*}{x} = 0.42 \left(Re_{\text{ref}}\right)^{-0.2775} \tag{8}$$

where the Reynolds number $Re_{\text{ref}} = \frac{\rho_{\text{ref}} u_\infty x}{\mu_{\text{ref}}}$ is based on Eckert's reference conditions [30], and x is measured from the origin of the radial flow. These correlations are implemented within HYPNOZE. For improved accuracy, the design code can also benefit from Navier-Stokes predictions in which case the viscous contour is gradually displaced from the inviscid one based on the local boundary layer displacement thickness predictions.

In the most downstream part of contoured nozzles, the rate of the nozzle boundary layer growth exceeds the one of the nozzle contour as illustrated in Fig. 7. As a result, the uniform inviscid core flow diameter

would shrink if nozzles were manufactured in whole. Substantial aerodynamic and economic gains can be achieved by cutting-off the nozzle at an optimized location which maximizes the uniform core flow [3, 31]. This optimization feature is also implemented in the code.

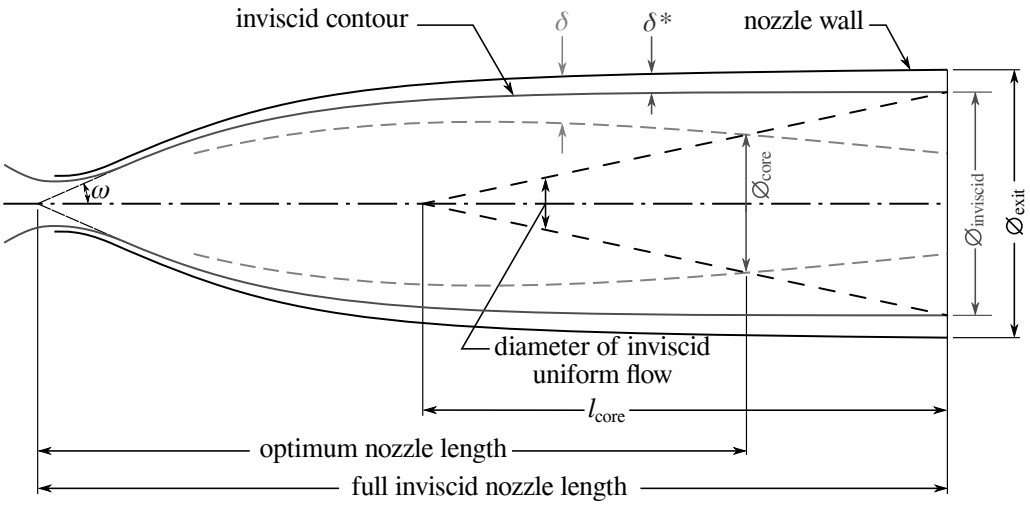

Fig 7. Effect of boundary layer on optimum nozzle length [31].

3. Validation of the nozzle design code

The HYPNOZE design code has been validated against predictions from an Euler solver. The methodology consists in generating an inviscid contour with the method of characteristics and to supply this contour to an numerical inviscid flow solver. Results are shown in Fig. 8 where the Mach number within the nozzle is depicted for the method of characteristics in the upper-half of the image (the values in the subsonic convergent being approximated from a simple area ratio rule), and for the Euler predictions in the lower-half. The excellent agreement achieved all across the domain indicates that the method of characteristics is correctly implemented within the present nozzle design code and that the accuracy offered by the second order scheme is sufficient. The weak variations observed within the Euler results in the uniform core are introduced by numerical errors and are actually emphasized by the choice of the particular contours.

Boundary layers developing along the nozzle contour are known [32] to lead to an improper cancellation of the characteristics, thereby influencing the nozzle flow expansion and its radial uniformity at the exit. It is shown in Fig. 9 that a good agreement for the Mach number across the nozzle may still be obtained in between the theoretical inviscid predictions from HYPNOZE and the Navier-Stokes ones provided that an appropriate viscous correction is used (even in presence of extremely thick boundary layers). For this nozzle designed for Mach 18, the Navier-Stokes predictions indicate a free-stream Mach number of 17.94 with a radial uniformity in the nozzle exit plane better than 0.4% without using the optimization procedures described by [33]. This serves to further demonstrate the accuracy of the HYPNOZE code together with appropriate viscous corrections in a real gas environment.

4. Influence of real gas effects on nozzle contours

In this paragraph, one considers an isentropic flow expansion of pure nitrogen from a stagnation pressure p_0=166MPa and a stagnation temperature T_0=2400K. The flow properties for such an expansion for different Mach numbers are indicated in Fig. 10. It is shown that the specific heat ratio of this gas at high pressure and high temperature is substantially lower (Fig. 10c) than the perfect gas value ($\gamma = 1.4$), and that the use of a real gas equation of state is indeed justified.

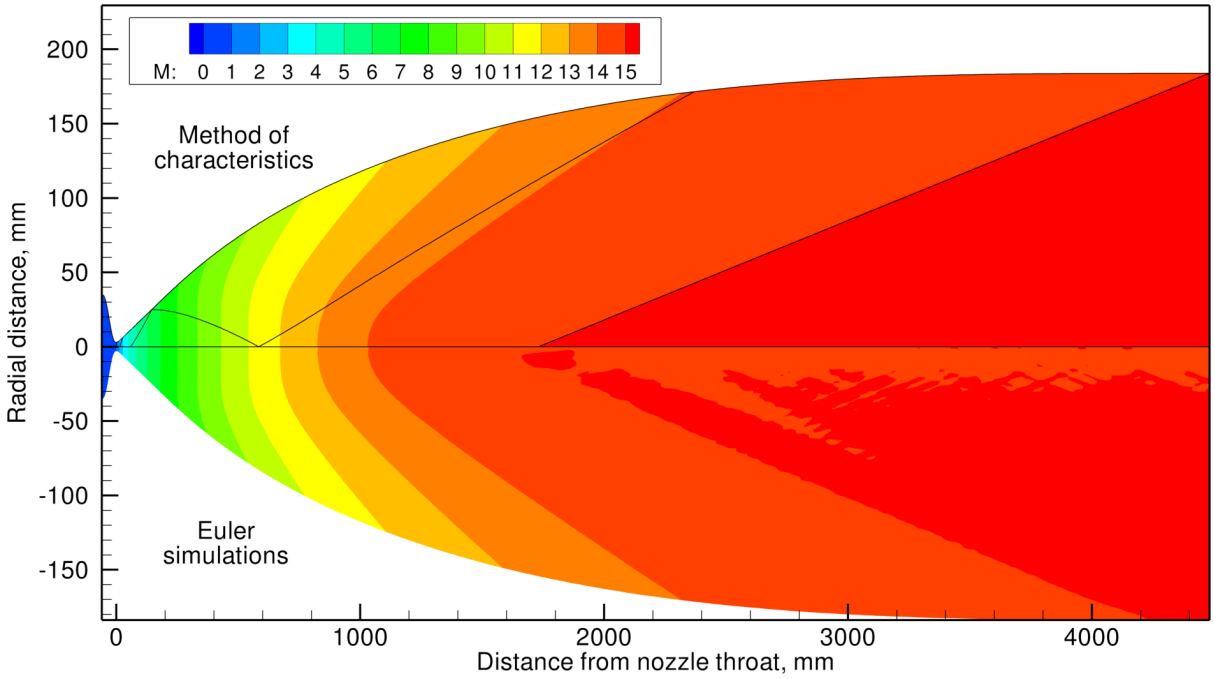

Fig 8. Validation of the HYPNOZE design code against results from an Euler flow solver (top-half: predictions from the method of characteristics using the present design code; bottom-half: Euler results).

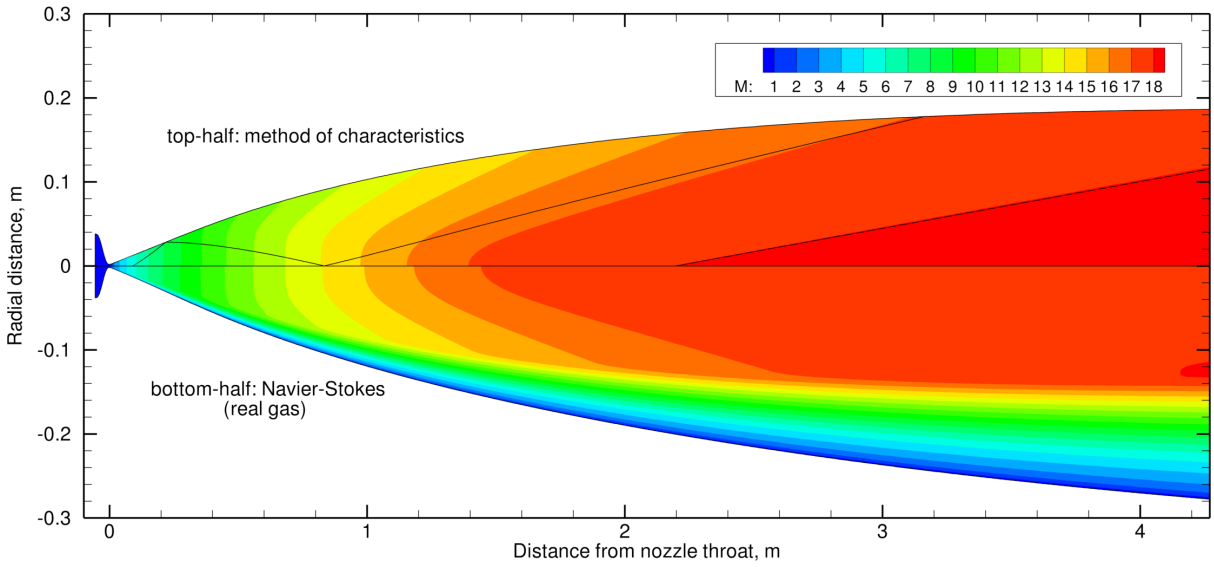

Fig 9. Mach number comparison between the theoretical predictions from HYPNOZE and the corresponding Navier-Stokes ones after correcting the inviscid contour for viscous effects.

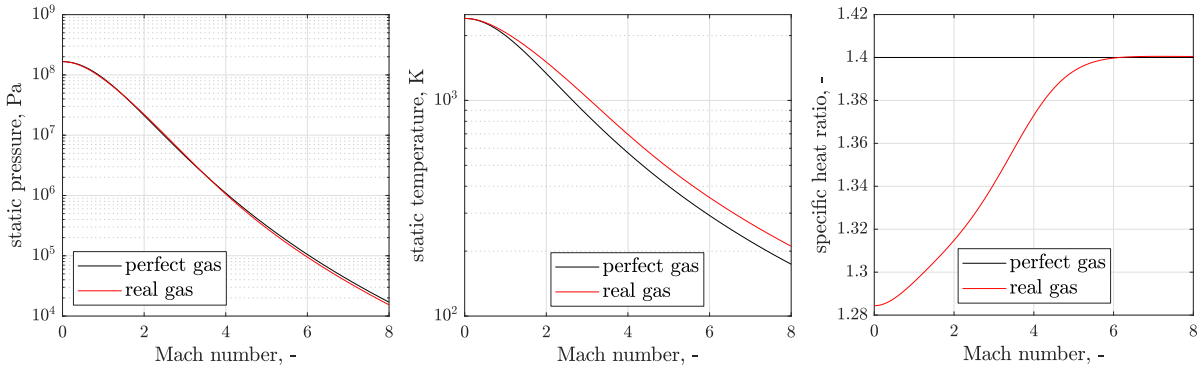

(a) Static pressure. **(b)** Static temperature. **(c)** Specific heat ratio.

Fig 10. Flow properties for an isentropic flow expansion starting from p_0=166MPa and T_0=2400K, assuming either a perfect gas equation of state or a real gas one [19].

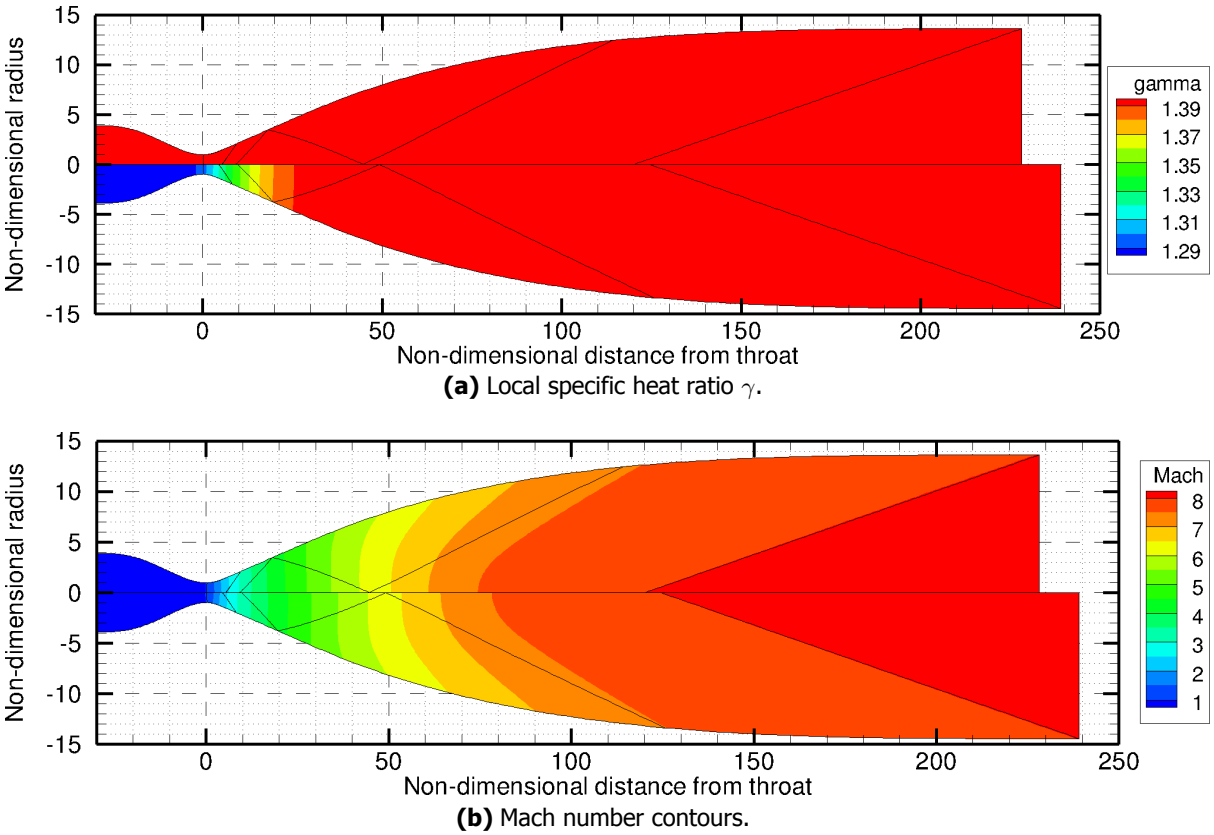

(a) Local specific heat ratio γ.

(b) Mach number contours.

Fig 11. Influence of the equation of state on the inviscid contour of Mach 8 contoured nozzles for nitrogen. The top-half of each figure is for perfect gas designs, whereas the bottom-half is for real gas designs.

The corresponding tabulated flow properties (and others) may be used to design a contoured nozzle using HYPNOZE. As shown in Fig. 11 for Mach 8 nozzles ($\omega = 9°$, $R = 30$, $X_{BC} = 12$), the location of the different points bounding the radial flow region (E, G, A, B as defined in Fig. 1) differ slightly whether a perfect gas equation of state (top-half nozzle) or a real gas one (bottom-half nozzle) are used. This is due to the influence of the variable isentropic exponent on the flow properties within the radial flow region. The resulting inviscid nozzle contour built around this region following the method described earlier is also influenced. The most noticeable variations are observed on the nozzle length and nozzle exit diameter, both of them being larger than the reference perfect gas case when variations of the isentropic exponent are accounted for (Fig. 11a). For the present design parameters, the area ratio $\frac{A_{\text{exit}}}{A^*}$ increases from 190.1 for a perfect gas (as expected from theory) to 213.5 when real gas effects are accounted for. The corresponding Mach number contours across the nozzle are shown in Fig. 11b. Whether a perfect gas equation of state or a real one are used, a uniform parallel flow region is always obtained at the nozzle exit. This is consistent with the assumptions used for each design, but in practice the real gas inviscid contour is expected to be more relevant since it accounts for more physics.

5. Parametric studies

The HYPNOZE design code is efficient and robust enough to enable scripted parametric studies on the main design parameters presented in §2.1. Typical results obtained by varying the nozzle opening angle ω and the transition length X_{BC} are presented in Fig. 12 showing the dimensions of the core flow and the length of the optimized nozzle as the parameters ω and X_{BC} are altered.

Dimensional constraints (i.e. minimum desirable core flow dimensions, the maximum nozzle length, and the minimum advised distance between points B and C as expressed by [5]) have been added to these results to show which design parameters will lead to an acceptable nozzle configuration. Other design parameters could be varied as well (such as the nozzle throat diameter), and other characteristic dimensions could also be looked at, such as the nozzle exit diameter.

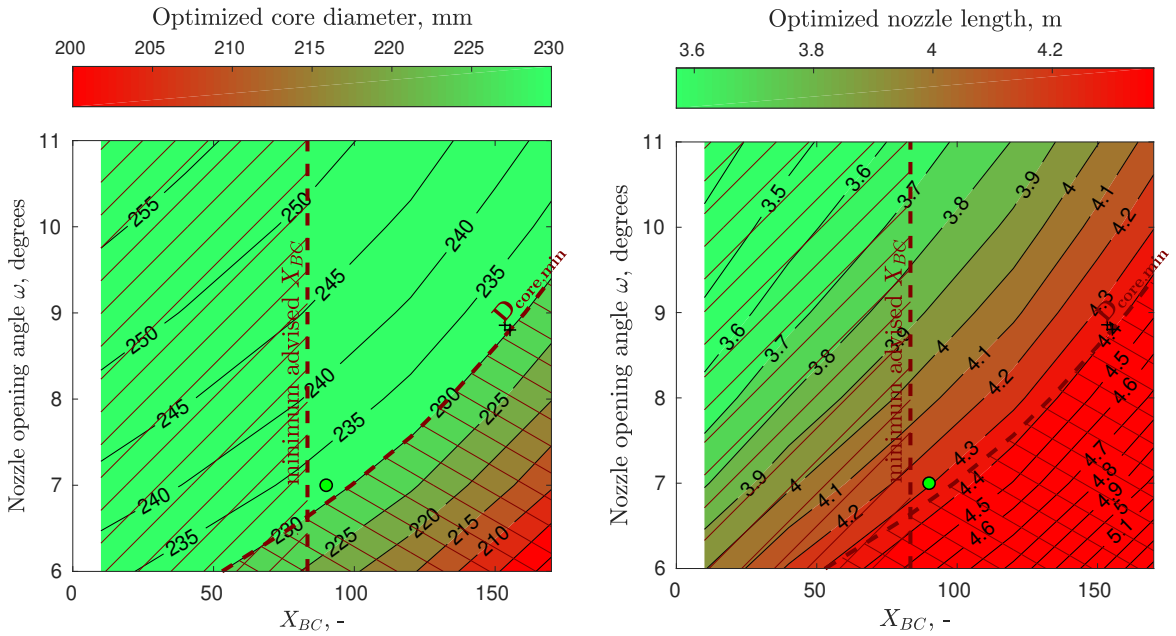

(a) Optimized core flow diameter.

(b) Optimized nozzle length.

Fig 12. Example of parametric studies performed for a real gas Mach 18 nozzle varying ω and X_{BC} (other design parameters are kept constant with R_c=30 and r^*=1.85mm) and starting from p_0 =166MPa and T_0 =2400K.

6. Summary and perspectives

A design methodology for axisymmetric supersonic and hypersonic contoured nozzles has been presented and validated. It relies on tabulated flow properties obtained from either perfect or real gas equations of state, and can therefore be applied to a wide range of test gases and stagnation flow conditions provided suitable equations of state are available. Special attention has been paid to the treatment of the transonic region in the specific case of real gases in order to ensure continuity of the first and second derivatives all along the contour. The design tool also includes design methods for the subsonic convergent and features viscous corrections. The influence of real gas effects on the nozzle area ratio has been demonstrated, with larger values typically required to reach a given free-stream Mach number.

The HYPNOZE tool currently enables to design contoured nozzles from low supersonic to hypersonic Mach numbers for various test gases using either a perfect gas or a real gas equation of state. As for the future, it would be relevant to couple it with the DEKAF boundary layer code [34, 35] and the VESTA stability code [36] in order to accurately compute the boundary layer profiles all along the nozzle walls and their stability. This would further improve the accuracy of the viscous correction for a fraction of the computational cost required by full Navier-Stokes computations, and would prove particularly useful for the design and optimization of quiet nozzles, among others. It could also be extended to enable the design of planar nozzles.

Acknowledgments

This activity has been partially supported by ESA, through Contract No. 4000114170/15/NL/KML. The main author would like to thank J. Marandé and F. Lozano for the improvements brought to the nozzle design code during their internships, and Z. Ilich for kindly reviewing the manuscript.

References

[1] L. Prandtl and A. Busemann. Näherungsverfahren zur zeichnerischen Ermittlung von ebenen Strömungen mit Überschallgeschwindigkeit. In *Stodola Festschrift*, page 499, 1929.

[2] I. E. Beckwith, H. W. Ridyard, and N. Cromer. The aerodynamic design of high Mach number nozzles utilizing axisymmetric flow with application to a nozzle of square test section. Technical Note TN 2711, National Advisory Committee for Aeronautics, June 1952.

[3] Y.-N. Yu. A summary of design techniques for axisymmetric hypersonic wind tunnels. In *AGARDograph35*. NATO, November 1958.

[4] J. C. Sivells. Aerodynamic design of axisymmetric hypersonic wind tunnel nozzles. *Journal of Spacecraft and Rockets*, 7(11):1292–1299, November 1970.

[5] J. C. Sivells. A computer program for the aerodynamic design of axisymmetric and planar nozzles for supersonic and hypersonic wind tunnels. Technical Report AEDC-TR-78-63, Arnold Engineering Development Center, December 1978.

[6] A. H. Shapiro. *The dynamics and thermodynamics of compressible fluid flow*, volume I. The Ronald Press Company, 1954.

[7] J. D. Anderson. *Modern compressible flow: With historical perspective*. McGraw-Hill, 3rd edition, 2004.

[8] A. Ferri. *Elements of aerodynamics of supersonic flow*. Macmillan Co., 1949.

[9] K. Foelsch. A new method of designing two dimensional Laval nozzles for a parallel and uniform jet. Technical Report Report NA-46-235-2, North American Aviation, May 1946.

[10] R. J. Cresci. Tabulation of coordinates for hypersonic axisymmetric nozzles. Part 1: Analysis and coordinates for test section Mach numbers of 8, 12 and 20. Technical Report TN 58-300, Aeronautical Research Laboratory, October 1958.

[11] J. J. Korte. Inviscid design of hypersonic wind tunnel nozzles for a real gas. In *8th AIAA Aerospace Science Meeting*, number AIAA paper 2000-0677, 2000.

[12] K. Hannemann. Design of an axisymmetric, contoured nozzle for the HEG. Technical Report NASA STI/Recon Technical Report N, 90, 28812, DLR, 1990.

[13] K. M. Chadwick, M. S. Holden, and J. J. Korte. Design and fabrication of a Mach 8 contoured nozzle for the LENS facility. In *34th AIAA Aerospace Sciences Meeting and Exhibit*, number AIAA paper 1996-0585, January 1996.

[14] E. Costilow Guentert and H. E. Neumann. Design of axisymmetric exhaust nozzles by method of characteristics incorporating a variable isentropic exponent. Technical Report NASA TR R-33, NASA, 1959.

[15] C. B. Johnson, L. R. Boney, J. C. Ellison, and W. D. Erickson. Real-gas effects on hypersonic nozzle contours with a method of calculation. Technical Note NASA TN D-1622, NASA Langley Research Center, April 1963.

[16] G. Simeonides. Design of a Mach 15 axisymmetric nozzle. Internal Note 82, von Karman Institute for Fluid Dynamics, March 1987.

[17] F. L. Shope. Contour design techniques for super/hypersonic wind tunnel nozzles. In *24th AIAA Applied Aerodynamic Conference*, number AIAA paper 2006-3665, June 2006.

[18] S. P. Schneider. Fabrication and testing of the Purdue Mach-6 quiet-flow Ludwieg tube. In *38th AIAA Aerospace Sciences Meeting & Exhibit*, number AIAA paper 2000-0295, January 2000.

[19] R. Span, E. W. Lemmon, R. T Jacobsen, and W. Wagner. A reference quality equation of state for nitrogen. *International Journal of Thermophysics*, 19(4):1121–1132, 1998.

[20] I. M. Hall. Transonic flow in two-dimensional and axially-symmetric nozzles. *Quarterly journal of Mechanics and Applied Mathematics*, XV(4):487–508, 1962.

[21] J. R. Kliegel and J. N. Levine. Transonic flow in small throat radius of curvature nozzles. *AIAA Journal*, 7(7):1375–1378, July 1969.

[22] C. S. Craddock. *Computational optimization of scramjets and shock tunnel nozzles*. PhD thesis, The University of Queensland, August 1999.

[23] F. L. Shope and M. E. Aboulmouna. On the importance of contraction design for supersonic wind tunnel nozzles. In *26th AIAA Aerodynamic measurement technology and ground testing conference*, number AIAA paper 2008-3940, June 2008.

[24] I. E. Beckwith. Development of a high Reynolds number quiet tunnel for transition research. *AIAA Journal*, 13(3):300–306, March 1975.

[25] S. P. Schneider. Development of hypersonic quiet tunnels. *Journal of Spacecraft and Rockets*, 45(4):641–664, July-August 2008.

[26] M. T. Lakebrink, K. G. Bowcutt, T. Winfree anf C. C. Huffman, and T. J. Juliano. Optimization of a Mach-6 quiet wind-tunnel nozzle. *Journal of Spacecraft and Rockets*, 55(2):315–321, March 2018.

[27] F.-J. Chen, S. P. Wilkinson, and I. E. Beckwith. Görtler instability and hypersonic quiet nozzle design. *Journal of Spacecraft and Rockets*, 30(2):170–175, March-April 1993.

[28] E. C. Anderson and C. H. Lewis. Laminar or turbulent boundary-layer flows of perfect gases or reacting gas mixtures in chemical equilibrium. Technical Report NASA-CR-1893, NASA, October 1971.

[29] E. E. Edenfield. Contoured nozzle design and evaluation for hotshot wind tunnels. In *3rd AIAA Aerodynamic testing conference*, number AIAA paper 1968-0369, April 1968.

[30] E. R. G. Eckert. Engineering relations for heat transfer and friction in high-velocity laminar and turbulent boundary-layer flow over surfaces with constant pressure and temperature. *Transactions of the ASME*, 78(6):1723–1283, August 1956.

[31] J. Lukasiewicz. *Experimental methods of hypersonics*. Marcel Dekker, Inc, 1973.

[32] G. Candler and J. Perkins. Effects of vibrational nonequilibrium on axisymmetric hypersonic nozzle design. In *29th AIAA Aerospace Sciences Meeting*, number AIAA paper 1991-0297, January 1991.

[33] J. J. Korte. Aerodynamic design of axisymmetric hypersonic wind-tunnel nozzles using a least-squares/parabolized Navier-Stokes procedure. *Journal of Spacecraft and Rockets*, 29(5):685–690, September-October 1992.

[34] K. J. Groot, F. Miró Miró, E. S. Beyak, A. Moyes, F. Pinna, and H. L. Reed. DEKAF: spectral multi-regime basic-state solver for boundary layer stability. In *AIAA Aviation*, number AIAA paper 2018-3380, June 2018.

[35] F. Miró Miró, E. S. Beyak, D. Mullen, F. Pinna, and H. Reed. Ionization and dissociation effects on hypersonic boundary-layer stability. In *31st Congress of the International Council of the Aeronautical Sciences*, number 837, September 2018.

[36] F. Pinna. VESTA toolkit: a software to compute transition and stability of boundary layers. In *43rd AIAA Fluid Dynamics Conference*, number AIAA paper 2013-2616, June 2013.